ISPRS Journal of Photogrammetry and Remote Sensing 66 (2011) 146–152

Contents lists available at ScienceDirect

ISPRS Journal of Photogrammetry and Remote Sensing

journal homepage: www.elsevier.com/locate/isprsjprs

Ground settlement monitoring based on temporarily coherent points between two SAR acquisitions

Lei Zhang [a], Xiaoli Ding [a,*], Zhong Lu [b]

[a] Department of Land Surveying and Geo-Informatics, The Hong Kong Polytechnic University, Hung Hom, KLN, Hong Kong
[b] US Geological Survey, Vancouver, WA, USA

ARTICLE INFO

Article history:
Received 15 June 2009
Received in revised form
12 October 2010
Accepted 13 October 2010
Available online 10 November 2010

Keywords:
SAR
Monitoring
Statistics
Change detection
Comparison

ABSTRACT

An InSAR analysis approach for identifying and extracting the temporarily coherent points (TCP) that exist between two SAR acquisitions and for determining motions of the TCP is presented for applications such as ground settlement monitoring. TCP are identified based on the spatial characteristics of the range and azimuth offsets of coherent radar scatterers. A method for coregistering TCP based on the offsets of TCP is given to reduce the coregistration errors at TCP. An improved phase unwrapping method based on the minimum cost flow (MCF) algorithm and local Delaunay triangulation is also proposed for sparse TCP data. The proposed algorithms are validated using a test site in Hong Kong. The test results show that the algorithms work satisfactorily for various ground features.

1. Introduction

Temporal decorrelation is a major limitation for the application of interferometric synthetic aperture radar (SAR) (InSAR) (e.g. Zebker and Villasenor, 1992; Lu et al., 2005). Persistent Scatterer (PS) Interferometry (PSI), an extension to the conventional InSAR, is a proven effective technique for measuring the displacement in areas of low correlation. Since Ferretti et al. (1999) first suggested an algorithm to exploit PS pixels, similar algorithms have been developed by various groups. These methods identify PS from an interferogram time-series either using a functional temporal model (Ferretti et al., 2000; Colesanti et al., 2003; Werner et al., 2003) or the spatial correlation of phase measurements (Hooper et al., 2004). However all these methods can only obtain reliable deformation measurements in regions with enough SAR acquisitions. In areas where the number of interferograms does not meet the minimum requirement, the methods usually fail to identify a dense network of PS pixels. The Signal-to-Clutter Ratio (SCR) (Adam et al., 2004) is another type of method for PS identification that requires a spatial estimation window around a point scatterer. The method does not need to calibrate the amplitude data to estimate the SCR and it does not require many SAR images.

Although the accurate coregistration of PS is critical in PSI, there is usually no special consideration for PS precise coregistration in current PSI methods. All the slave SAR images are typically coregistered to a single master SAR image based on the range and azimuth offsets of distributed windows over the images. However, since the majority (typically 90% or more) of the pixels in the images are distributed scatterers (non-PS pixels) (Kampes, 2006) and the errors in their estimated offsets are in general larger than those in the estimated offsets of PS, the coregistration accuracy of PS has a potential risk of being affected by the unoptimizable coregistration methods.

In this paper an InSAR analysis approach is presented. It includes algorithms for identifying and coregistering the coherent points between two SAR acquisitions, named as temporarily coherent points (TCP), and for determining motions of TCP for applications such as ground settlement monitoring. The identification of TCP is based on the standard deviation of the estimated offsets derived by Bamler (2000) and the fact that the offsets estimated from strong scatterers are less sensitive to the window size and oversampling factor used than those from distributed scatterers. The approach is validated using a test site located in Hong Kong.

2. Methodology

2.1. Offsets estimation

Estimation of the offsets between two SAR images with an accuracy of better than about 1/10 of a pixel is critical in interferogram generation to avoid significant loss of phase

* Corresponding author. Tel.: +852 2766 5965; fax: +852 2330 2994.
E-mail address: lsxlding@polyu.edu.hk (X. Ding).

0924-2716/$ – see front matter © 2010 International Society for Photogrammetry and Remote Sensing, Inc. (ISPRS). Published by Elsevier B.V. All rights reserved.
doi:10.1016/j.isprsjprs.2010.10.004

coherence (Hanssen, 2001). Several factors contribute to image offsets, including different timing along the satellite orbit, baseline variation, pulse repetition frequency (PRF) variation, ground deformation and varying satellite velocity (Ferretti et al., 2007). Offsets between a pair of SAR images can be typically described by such geometric changes between the two images as range and azimuth shifts, range and azimuth stretches, and range and azimuth skews. The effects of stretch and skew are limited for ERS and Envisat data (Gatelli et al., 1994). In theory the offsets are also related to local ground elevation although the offsets from this effect are insignificant for ERS and Envisat data due to the limited bandwidth of the data (Arikan et al., 2007).

The commonly used methods for estimating offsets between two SAR images are based either on cross-correlation between the two amplitude images (Gray et al., 1998; Rott et al., 1998; Michel and Rignot, 1999) or on a fringe visibility (also referred to as coherence optimization) algorithm (Derauw, 1999) that is mainly suitable for images of high coherence. For image pairs with long baselines the geometrical approach aided by reference DEM and orbit information (Fornaro et al., 2005) can also be considered. In the amplitude correlation method, the estimation of the local image offsets is reliable only when the features in the two SAR image patches are nearly identical (Strozzi et al., 2002). Therefore unstable features usually make the offsets vary randomly. This property will be used in the algorithm for TCP identification to be presented below.

2.2. Identification of TCP

As discussed above, the effects of stretch and skew can be neglected for ERS and Envisat data in image offset estimation. Therefore for areas undergoing gentle deformation the offsets estimated from patches of images with stable ground features should be nearly identical. For image patches with unstable ground features, on the other hand, the location of the correlation peak varies, leading to random changes in the estimated offsets. Fig. 1 shows the estimated offset vectors for an area over the Hong Kong Airport. It can be seen from the results that after removing the initial offsets estimated based on the satellite orbits the remaining offsets in the sea and in the mountainous areas appear very random due to errors in the estimated offsets while the offsets of the strong scatterers are very consistent (red dots without apparent offset vectors). It is therefore possible to distinguish stable image patches (coherent scatterers) from the unstable ones (distributed targets) based on the offset information.

The estimated offsets of stable image patches are less sensitive to the size of the patches and to the oversampling factor. This property can also be verified theoretically (Bamler, 2000). When estimating the offsets with the cross-correlation method, the standard deviation of an estimated offset $\delta_{r,a}$ (in range or azimuth) for a homogenous image patch is

$$\sigma(\delta_{r,a}) = \sqrt{\frac{3}{2N}} \cdot \frac{\sqrt{1-\gamma^2}}{\pi\gamma} \chi^{\frac{3}{2}} \tag{1}$$

where σ is the standard deviation expressed as a fractional number of pixels; N is the number of samples in a patch; γ is the coherence of the patch that is also related to N as

$$|\hat{\gamma}| = \frac{\left| \sum_{i=1}^{m}\sum_{j=1}^{n} s_1(i,j)s_2^*(i,j) \right|}{\sqrt{\sum_{i=1}^{m}\sum_{j=1}^{n} s_1(i,j)s_1^*(i,j) \sum_{i=1}^{m}\sum_{j=1}^{n} s_2(i,j)s_2^*(i,j)}}. \tag{2}$$

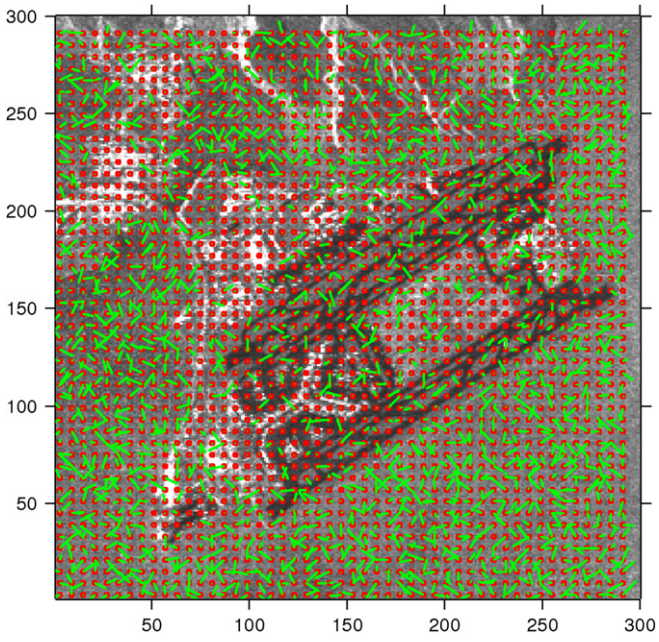

Fig. 1. Offset vectors over the area of Hong Kong Airport as determined by the method of cross correlation where the red circles are the sampled points and the green arrows are the offset vectors. The window size and the oversampling factor used are 5 × 25 and 2, respectively. The initial offsets determined based on the satellite orbits were first removed before this estimation is carried out. The points are sampled every 6 and 30 pixels in the range and azimuth directions for better visualization.

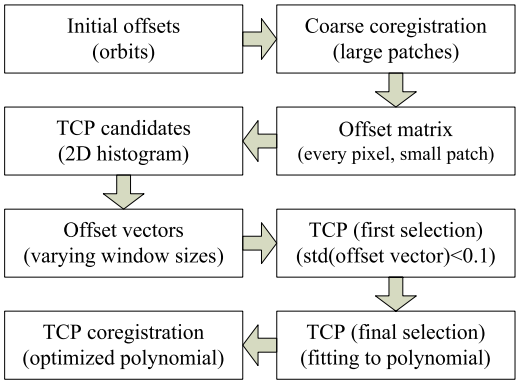

Fig. 2. Block diagram of the proposed method for coherent point identification.

$N = m \times n$, and χ is the oversampling factor. It should be noted that although Eq. (1) was derived for image patches with distributed scatterers, it can be taken as a higher bound for image patches dominated by strong scatterers (Serafino, 2006).

Although Eq. (1) may be biased for images with dominating scatterers, it can be used effectively to separate coherent scatterers from incoherent ones. The standard deviation calculated from Eq. (1) may vary significantly with the number of samples in areas with low coherence while it should be relatively stable in areas with high coherence. Therefore coherent scatterers may be identified by calculating and examining the offsets while changing the size of the image patches.

After calculating the initial image offsets based on satellite orbits, first, the proposed method for identifying TCP starts by dividing the scene into a set of large patches (e.g., 256 × 256) and the range and the azimuth offsets of each of the patches are estimated and used to determine the coefficients of an offset polynomial. Second, the estimated offsets are used as initial inputs and the method of cross-correlation is applied at every pixel using

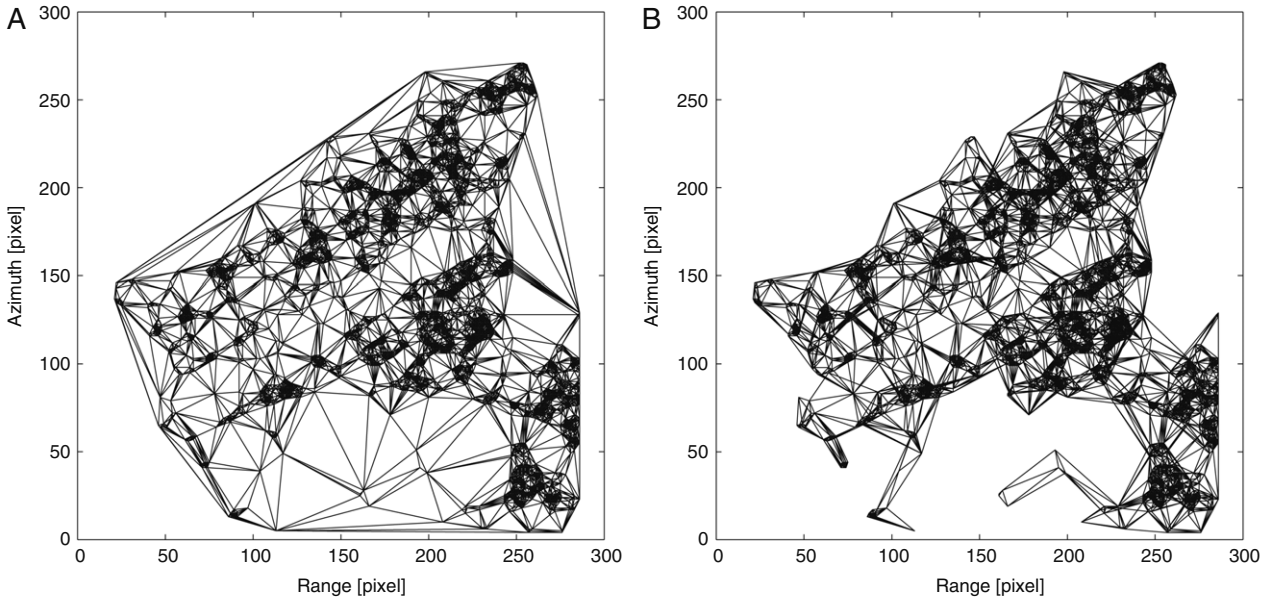

Fig. 3. Comparison of different Delaunay triangulation networks. (A) TCP connected by global Delaunay triangulation; (B) TCP connected by local Delaunay triangulation.

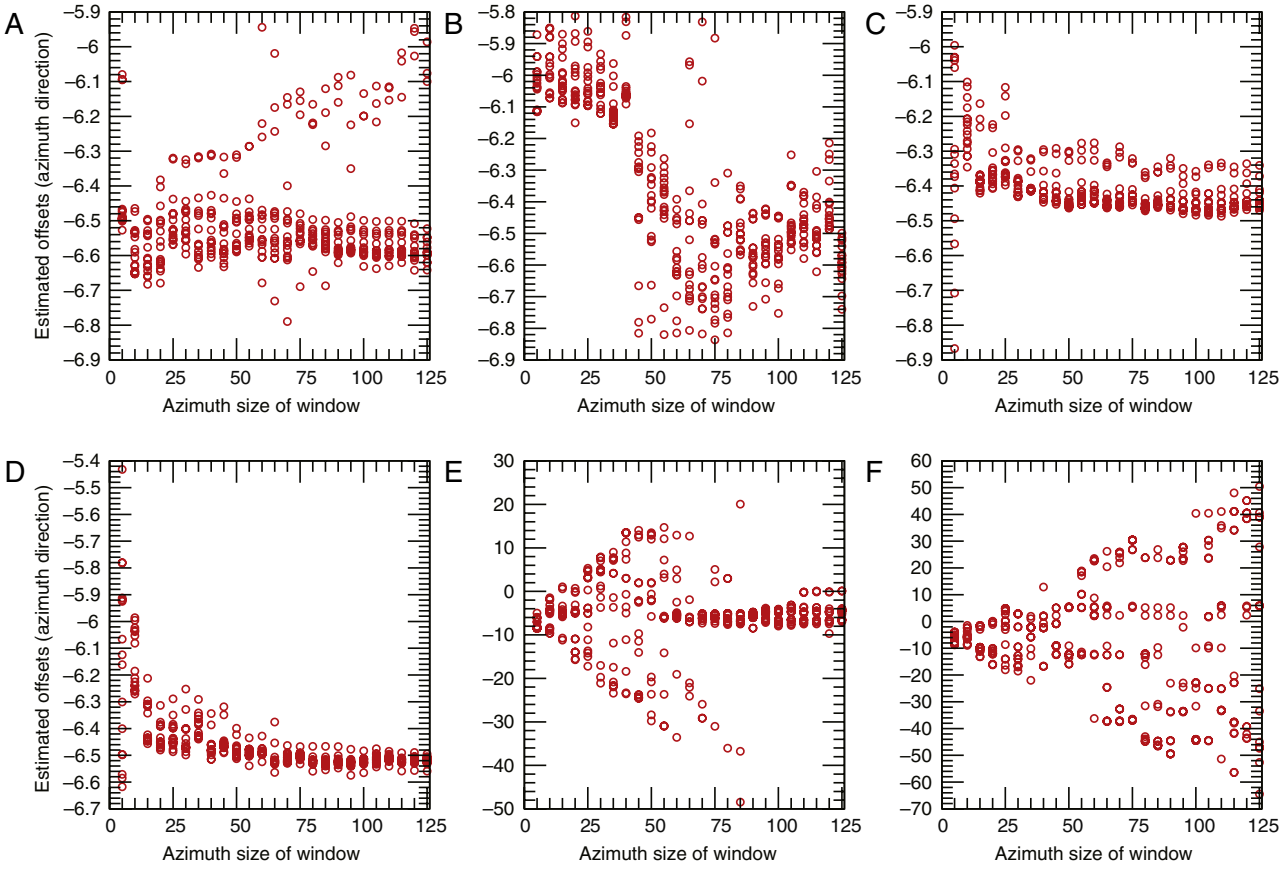

Fig. 4. Estimated azimuth offsets of two CR and other types of scatterers. The window size varies from 5-by-5 to 125-by-125 in the offset estimation. (A) CR1; (B) CR2; (C) Building point 1; (D) Building point 2; (E) Hill point; (E) Sea point.

smaller patches (e.g., 5×5). An offset matrix can be obtained from the estimated offset values,

$$O_{l\times m} = \begin{bmatrix} o_{1,1} & o_{1,2} & \cdots & o_{1,m} \\ o_{2,1} & o_{2,2} & \cdots & o_{2,m} \\ \vdots & \vdots & & \vdots \\ o_{l,1} & o_{l.2} & \cdots & o_{l,m} \end{bmatrix} \tag{3}$$

where $o_{i,j}$, $i = 1, 2, \ldots, l$; $j = 1, 2, \ldots, m$ is the offset of pixel (i, j), which contains the offset components in both the azimuth and the range directions.

The pixels with identical offsets are selected as TCP candidates using a 2-D histogram,

$$\begin{aligned} &o_c = peak\{hist_{2D}(O_{l\times m})\} \\ &|o_{i,k} - o_c| < A \end{aligned} \tag{4}$$

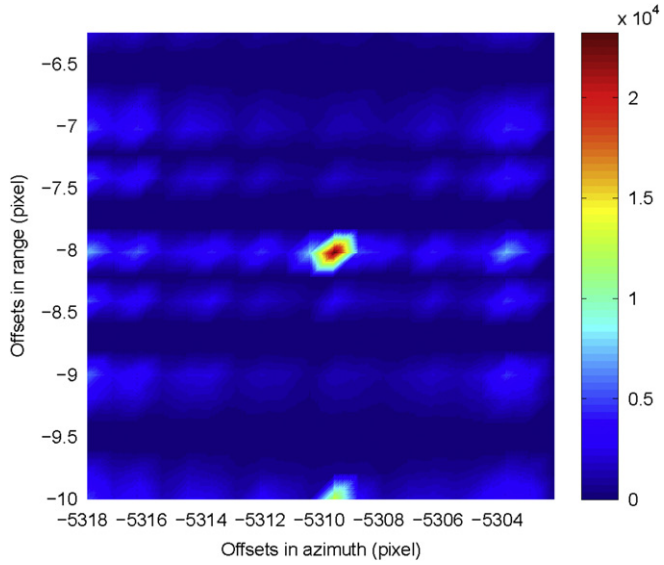

Fig. 5. 2D histogram of offsets at all pixels estimated using a window size of 3×15. The colour indicates the number of pixels whose offsets in range and azimuth direction locate in the corresponding intervals.

where A is the tolerance interval. To ensure most of the strong scatterers to be selected as TCP candidates, A can be set to 1. The 2-D histogram gives statistics on the consistency of the offsets with a tolerance threshold value determined based on the quickhull algorithm (Barber et al., 1996) that improves the computational efficiency significantly compared with the iterative search method. Third, the TCP candidates are further evaluated by changing the size of the image patches in cross-correlation estimation (e.g., from 5×5 to 125×125) and the oversampling factor to find the sub-pixel offsets. A fixed oversampling factor can be used for simplicity. A set of offsets can be obtained accordingly for any given TCP candidate (j). The TCP candidates whose offset standard deviations are smaller than 0.1 pixels are selected,

$$\begin{aligned} &OT_j = [ot_{j1}\ ot_{j2}\ \cdots\ ot_{jN}] \\ &std(OT_j) < 0.1. \end{aligned} \tag{5}$$

Fourth, the offsets of the TCP candidates are fit to a smooth polynomial and the TCP candidates whose offsets do not fit the polynomial well are discarded. The remaining candidates are finally selected as TCP. A 6-point truncated sinc interpolator kernel (Hanssen, 2001) is employed to resample TCP in the slave image based on the polynomial determined. A block diagram showing the procedure of selecting TCP is given in Fig. 2.

It is important to note that in the above process, since the cross-correlation is estimated each time from an image patch and a strong scatterer within a patch may dominate the cross-correlation estimation in several neighbouring patches, pixels near a stable scatterer may be mistakenly identified as TCP candidates. Although such errors should have been considerably reduced at the stage of sub-pixel offset estimation using very small image patches, pixels seriously affected by side lobes of strong scatterers may still be wrongly identified. The phase components of these points should mainly be from the neighbouring stable pixels so that they can be considered as one pixel. In addition, for the time series data analysis these points can be further removed based on the least squares residuals during the parameter estimation (i.e., DEM error and deformation rates) if the phases contain a large bias (Zhang et al., in press).

2.3. TCP phase unwrapping based on local Delaunay triangulation

The phase values of TCP, which are irregularly distributed, can be unwrapped after subtracting the topography phase. Delaunay triangulation has been widely used to connect such coherent scatterers to form a triangular network (Fig. 3(A)) (Costantini and Rosen, 1999). Delaunay triangulation defines a triangular network under the condition that all the circumcircles of all the triangles in the network are empty. The lengths of arcs in a Delaunay triangulation network are important as when an arc is long, the unwrapped phase difference between the two points concerned can easily exceed π, making phase unwrapping difficult. In addition, the atmospheric artefacts are strongly correlated in space (Zebker et al., 1997; Li et al., 2005, 2006). The differential atmospheric contributions between two nearby points are usually insignificant (e.g., usually lower than 0.1 rad for points less than 1 km apart) (Williams et al., 1998). The differential orbital errors also have similar properties. In order to reduce these errors, the TCP arcs should be limited, e.g., within 2 km. To this end we used a strategy of placing overlapping small regular patches over the image and connecting the TCP in each patch with Delaunay triangulation if the number of the TCP in the patch is no less than 3. One example of the proposed Delaunay triangulation network is shown in Fig. 3(B), where long arcs were effectively avoided. The patches are then unwrapped separately with the minimum cost flow (MCF) algorithm that solves for the flow along the arcs in each patch to minimize the network cost (Costantini, 1998; Chen and Zebker, 2001). The unwrapped patches are combined by comparing the phase values in the overlapping areas.

3. Experiments

3.1. Validation of the method for TCP identification

The proposed TCP selection method is validated with two corner reflectors (CRs), two buildings, and two distributed scatterers in Hong Kong. The locations of the objects in the radar coordinate system are carefully determined and the proposed method is then applied. For simplicity, when calculating the offsets of the points a fixed oversampling factor of 2 is used and the window size is changed from 5×5 to 125×125. The offsets of the points in the azimuth direction are shown in Fig. 4, where the offsets of the CRs as well as the two buildings appear to be consistent on a pixel level but considerable dispersion within one pixel can also be observed, indicating that the quality of the coherent points are different. On the other hand, due to the change in the surface features between the two SAR acquisitions, offsets estimated for the point in the sea and that on the hill fluctuate randomly for up to 60 pixels. The results from these typical scatterers have shown that the proposed method can identify coherent points successfully.

3.2. Settlement determination

Since most of the land occupied by the Hong Kong Airport was reclaimed from the sea, ground settlement in the area has been expected. A pair of Envisat ASAR images acquired in April 2006 and March 2007 with a perpendicular baseline of 44 m and time baseline of 315 days is used to determine the settlement in the area.

3.2.1. Comparison of point selection methods

The SCR threshold (Adam et al., 2004), the coherence threshold (Costantini and Rosen, 1999; Berardino et al., 2002; Mora et al., 2003; Lanari et al., 2004) and the newly proposed method (referred to as offset method hereafter for simplicity) are used for identifying coherent scatterers in the study area. For the offset method the

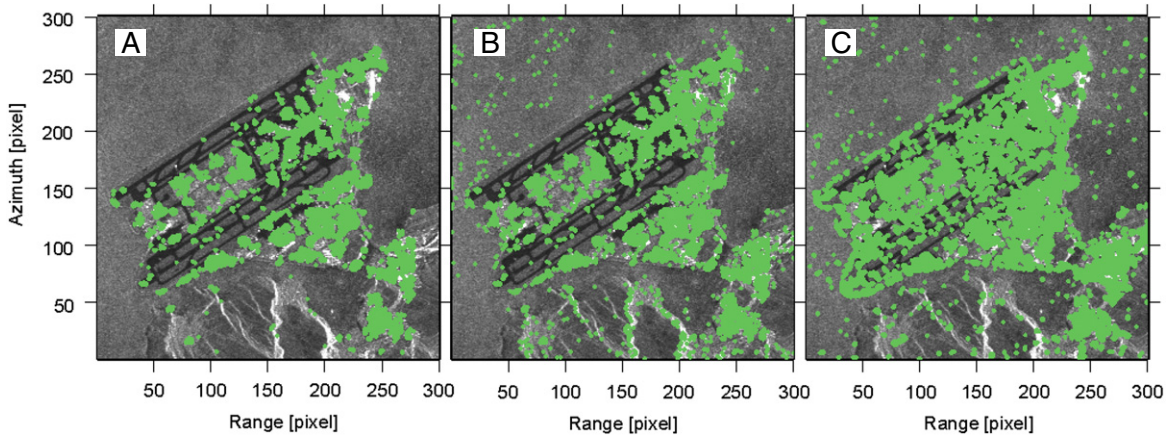

Fig. 6. Coherent scatterers identified with three different methods: (A) 5613 TCP identified with the offset method; (B) 7355 points identified with the SCR method when SCR > 2; and (C) 12,153 points identified with coherence method when the coherence threshold = 0.4 (coherence estimation window: 5 × 20).

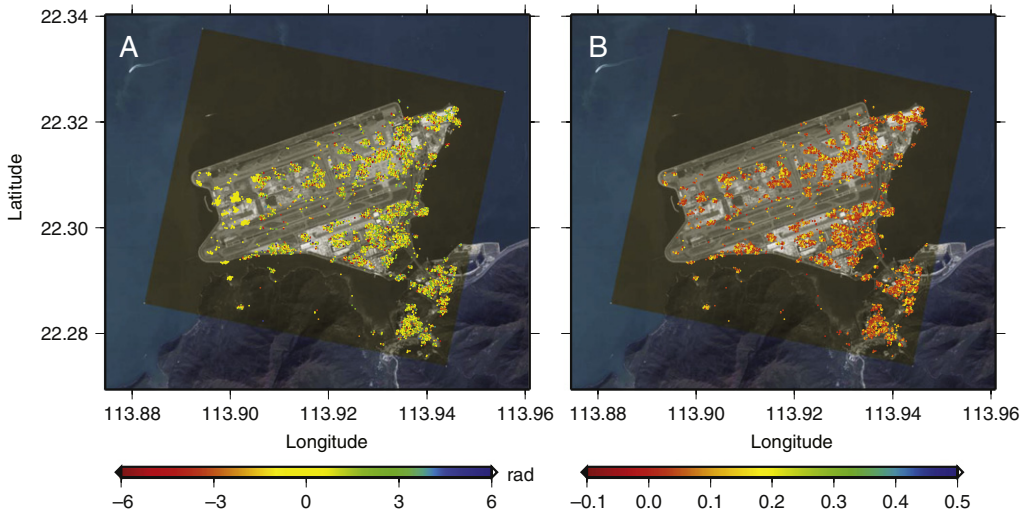

Fig. 7. (A) Phase differences between interferograms coregistered with different polynomials (unit: radian); and (B) Improvement in the coherence of the selected TCP when using the proposed coregistration strategy.

range and the azimuth offsets at every pixel are estimated using an image patch size of 3 × 15. The 2-D histogram of the estimated offsets is shown in Fig. 5, indicating that the consistent range and azimuth offsets are −8 pixels and −5310 pixels respectively. After a multilooking operation with a factor of 1 × 5, 5613 TCP are finally selected (Fig. 6(A)). When the SCR method is used, 7355 points are selected with the threshold value set to be SCR > 2 (Fig. 6(B)). 12153 points are selected with the coherence method (Fig. 6(C)), when the threshold is set to 0.4.

It can be seen from the results that all the three methods work well with strong scatterers. The number of points wrongly identified however varies considerably among the methods. Apparently the offset method works best in such unstable areas as in the sea as no points are wrongly selected.

3.2.2. TCP coregistration

The identified TCP are resampled according to the polynomial determined based on the offsets of the TCP (referred to as the TCP polynomial for simplicity). Errors in the polynomial will introduce phase noise as the polynomial gives the location of the TCP in the slave image where the interpolation kernel will be applied. For comparison, we also determined a polynomial with offsets from evenly distributed windows over the whole image and resampled the TCP with this polynomial (referred to as the global polynomial for simplicity). It is found that the interferometric phases of the resampled TCP from the two polynomial approaches are different (Fig. 7(A)). The phase differences have a mean of 0.25 rad and a standard deviation of 2.3 rad. Since the global polynomial was estimated from offsets on distributed windows over the whole image where most of the pixels are distributed scatterers, the offsets from the distributed scatterers are unreliable and can affect the polynomial determination, resulting in errors in the polynomial and phase noise. Fig. 7(B) shows the improvement in coherence when the TCP polynomial is used.

3.2.3. Settlement calculation

The TCP are connected with a local Delaunay triangulation (limiting the arc lengths to within 2 km) and the minimum cost flow (MCF) algorithm is applied to calculate the broken-line flow according to the residues. The unwrapped phases of the TCP are then determined based on the flows. The motions of the TCP along the line of sight (LOS) direction are then computed from the unwrapped phases of the TCP (see Fig. 8). The results show that the largest settlement along the LOS direction over the period of the 315 days was about 8 mm at the central part of the airport. The average settlement of the TCP is about 2 mm. Although the results cannot be validated with ground truth in the absence of such data, the overall pattern of the settlement is consistent with results reported earlier (Ding et al., 2004).

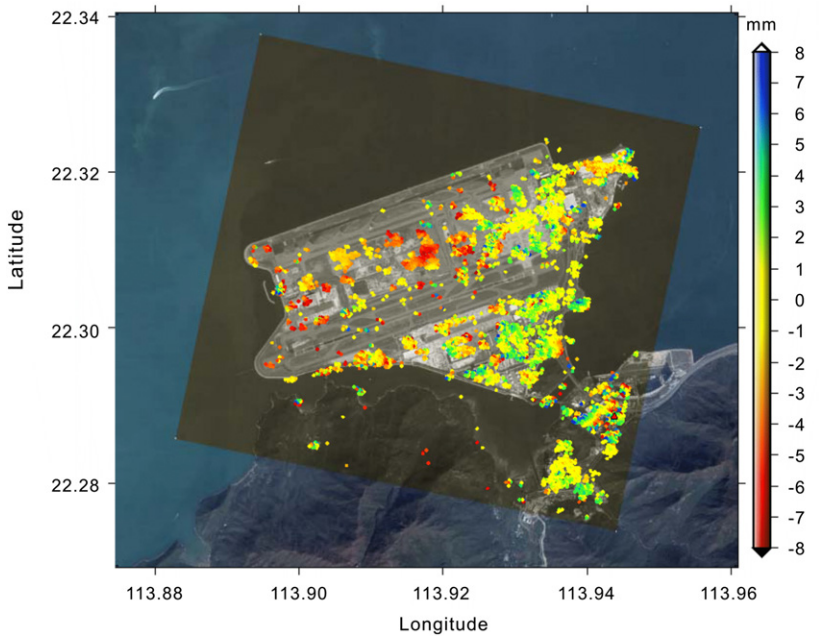

Fig. 8. Settlement of temporarily coherent points in LOS direction over April 2006–March, 2007 (unit: millimetre). Negative values indicate motion away from the satellite (i.e., settlement).

4. Conclusion

A method for identifying the temporarily coherent points (TCP) that exist between two SAR acquisitions has been presented. The method is useful in areas where the conventional differential InSAR technique does not work properly due to the decorrelation effects and where there are not enough SAR images to perform PSI analysis. An improved method for coregistering TCP has been proposed by estimating the offset polynomial based on the TCP offsets only. To unwrap the phase of the TCP reliably, a local triangulation strategy that limits the lengths of the arcs has been proposed. The proposed algorithms have been validated using test sites in Hong Kong and applied to determine the settlement of the Hong Kong Airport area.

Acknowledgements

The authors would like to thank Prof. Olaf H.A. Hellwich and two anonymous reviewers for their constructive comments and suggestions. The first author is supported by a Ph.D. studentship offered by the Hong Kong Polytechnic University. The research was supported by the Research Grants Council (RGC) of the Hong Kong Special Administrative Region (project number: PolyU 5155/07E), and the Sustainable Urbanisation Research Fund (SURF) of the Faculty of Construction and Land Use, The Hong Kong Polytechnic University.

References

Adam, N., Kampes, B.M., Eineder, M., 2004. The development of a scientific persistent scatterer system: modifications for mixed ERS/ENVISAT time series. In: Proc. ENVISAT/ERS Symposium, Salzburg, Austria, 6–10 September (on CD-ROM).

Arikan, M., van Leijen, F., Liu, G., Hanssen, R., 2007. Improved image alignment under the influence of elevation. In: Proc. Fringe 2007 Workshop, Frascati, Italy, 26–30 November (on CD-ROM).

Bamler, R., 2000. Interferometric stereo radargrammetry: absolute height determination from ERS-ENVISAT interferograms. In: IEEE Proc. IGARSS, vol. 2, Honolulu, HI, USA, 24–28 July, pp. 742–745.

Barber, C., Dobkin, D.P., Huhdanpaa, H., 1996. The quickhull algorithm for convex hulls. ACM Transactions on Mathematical Software (TOMS) 22 (4), 469–483.

Berardino, P., Fornaro, G., Lanari, R., Sansosti, E., 2002. A new algorithm for surface deformation monitoring based on small baseline differential SAR interferograms. IEEE Transactions on Geoscience and Remote Sensing 40 (11), 2375–2383.

Chen, C., Zebker, H., 2001. Two-dimensional phase unwrapping with use of statistical models for cost functions in nonlinear optimization. Journal of the Optical Society of America 18 (2), 338–351.

Colesanti, C., Ferretti, A., Novali, F., Prati, C., Rocca, F., e Inf, D., 2003. SAR monitoring of progressive and seasonal ground deformation using the permanent scatterers technique. IEEE Transactions on Geoscience and Remote Sensing 41 (7), 1685–1701.

Costantini, M., 1998. A novel phase unwrapping method based on network programming. IEEE Transactions on Geoscience and Remote Sensing 36 (3), 813–821.

Costantini, M., Rosen, P., 1999. A generalized phase unwrapping approach for sparse data. In: IEEE Proc. IGARSS, Hamburg, Germany, 28 June–02 July 1999, pp. 267–269.

Derauw, D., 1999. DInSAR and coherence tracking applied to glaciology: the example of Shirase Glacier. In: Proc. ESA Fringe 1999, Liège, Belgium, 10–12 November. 8 P. (on CDROM).

Ding, X., Liu, G., Li, Z., Li, Z., Chen, Y., 2004. Ground subsidence monitoring in Hong Kong with satellite SAR interferometry. Photogrammetric Engineering and Remote Sensing 70 (10), 1151–1156.

Ferretti, A., Monti-Guarnieri, A., Prati, C., Rocca, F., 2007. InSAR Principles: Guidelines for SAR Interferometry Processing and Interpretation. ESA Publications, TM-19.

Ferretti, A., Prati, C., Rocca, F., 1999. Permanent scatterers in SAR interferometry. In: Proc. SPIE, Florence, Italy, 20 September 1999, pp. 139–145.

Ferretti, A., Prati, C., Rocca, F., di Elettronica, D., 2000. Nonlinear subsidence rate estimation using permanent scatterers indifferential SAR interferometry. IEEE Transactions on Geoscience and Remote Sensing 38 (5), 2202–2212.

Fornaro, G., Manunta, M., Serafino, F., Berardino, P., Sansosti, E., 2005. Advances in multipass SAR image registration. In: IEEE Proc. IGARSS, Seoul, South-Korea, 25–29 July, pp. 4832–4835.

Gatelli, F., Guamieri, A., Parizzi, F., Pasquali, P., Prati, C., Rocca, F., 1994. The wavenumber shift in SAR interferometry. IEEE Transactions on Geoscience and Remote Sensing 32 (4), 855–865.

Gray, A., Mattar, K., Vachon, P., Bindschadler, R., Jezek, K., Forster, R., Crawford, J., 1998. InSAR results from the RADARSAT antarctic mapping mission data: estimation of glacier motion using a simple registration procedure. In: IEEE Proc. IGARSS, vol. 3, Seattle, WA, USA, 06–10 July, pp. 1638–1640.

Hanssen, R.F., 2001. Radar Interferometry: Data Interpretation and Error Analysis. Kluwer Academic Publishers, Dordrecht, The Netherlands.

Hooper, A., Zebker, H., Segall, P., Kampes, B., 2004. A new method for measuring deformation on volcanoes and other natural terrains using InSAR persistent scatterers. Geophysical Research Letters 31 (23), 611–615.

Kampes, B.M., 2006. Radar Interferometry: Persistent Scatterer Technique. Springer, Dordrecht, The Netherlands.

Lanari, R., Mora, O., Manunta, M., Mallorqui, J., Berardino, P., Sansosti, E., 2004. A small-baseline approach for investigating deformations on full-resolution differential SAR interferograms. IEEE Transactions on Geoscience and Remote Sensing 42 (7), 1377–1386.

Li, Z., Ding, X., Huang, C., Wadge, G., Zheng, D., 2006. Modeling of atmospheric effects on InSAR measurements by incorporating terrain elevation information. Journal of Atmospheric and Solar-Terrestrial Physics 68 (11), 1189–1194.

Li, Z., Muller, J., Cross, P., Fielding, E., 2005. Interferometric synthetic aperture radar (InSAR) atmospheric correction: GPS, Moderate Resolution Imaging Spectroradiometer (MODIS), and InSAR integration. Journal of Geophysical Research 110 (B3), B03410.

Lu, Z., Masterlark, T., Dzurisin, D., 2005. Interferometric synthetic aperture radar study of Okmok volcano, Alaska, 1992–2003: magma supply dynamics and postemplacement lava flow deformation. Journal of Geophysical Research 110 (B2), B02403.

Michel, R., Rignot, E., 1999. Flow of Glaciar Moreno, Argentina, from repeat-pass shuttle imaging radar images: comparison of the phase correlation method with radar interferometry. Journal of Glaciology 45 (149), 93–101.

Mora, O., Mallorqui, J., Broquetas, A., 2003. Linear and nonlinear terrain deformation maps from a reduced set of interferometric SAR images. IEEE Transactions on Geoscience and Remote Sensing 41 (10), 2243–2253.

Rott, H., Stuefer, M., Siegel, A., Skvarca, P., Eckstaller, A., 1998. Mass fluxes and dynamics of Moreno glacier, southern Patagonia icefield. Geophysical Research Letters 25 (9), 1407–1410.

Serafino, F., 2006. SAR image coregistration based on isolated point scatterers. IEEE Geoscience and Remote Sensing Letters 3 (3), 354–358.

Strozzi, T., Luckman, A., Murray, T., Wegmuller, U., Werner, C., 2002. Glacier motion estimation using SAR offset-tracking procedures. IEEE Transactions on Geoscience and Remote Sensing 40 (11), 2384–2391.

Werner, C., Wegmuller, U., Strozzi, T., Wiesmann, A., 2003. Interferometric point target analysis for deformation mapping. In: IEEE Proc. IGARSS, vol. 7, Seattle, Toulouse, France, 21–25 July, pp. 4362–4364.

Williams, S., Bock, Y., Fang, P., 1998. Integrated satellite interferometry: tropospheric noise, GPS estimates and implications for interferometric synthetic aperture radar products. Journal of Geophysical Research-Solid Earth 103 (B11), 27, 051–27, 067.

Zebker, H.A., Rosen, P.A., et al., 1997. Atmospheric effects in interferometric synthetic aperture radar surface deformation and topographic maps. Journal of Geophysical Research 102 (B4), 7547–7563.

Zebker, H., Villasenor, J., 1992. Decorrelation in interferometric radar echoes. IEEE Transactions on Geoscience and Remote Sensing 30 (5), 950–959.

Zhang, L., Ding, X.L., Lu, Z., 2010. Modeling PSInSAR time series without phase unwrapping. IEEE Transactions on Geoscience and Remote Sensing, in press (doi:10.1109/TGRS.2010.2052625).